Pressure-induced electronic and magnetic phase transitions in a Mott insulator: Ti-doped Ca_{3}Ru_{2}O_{7} bilayer ruthenate

T. Zou, H. B. Cao, G. Q. Liu, J. Peng, M. Gottschalk, M. Zhu, Y. Zhao, J. B. Leão, W. Tian, Z. Q. Mao, and X. Ke

Pressure-induced electronic and magnetic phase transitions in a Mott insulator - Ti-doped $Ca_3Ru_2O_7$ bilayer ruthenate

T. Zou[1], H. B. Cao[2], G. Q. Liu[3], J. Peng[4,5], M. Gottschalk[1], M. Zhu[1], Y. Zhao[6,7], J. B. Leão[6],

W. Tian[2], Z.Q. Mao[4], X. Ke[1*]

[1.] *Department of Physics and Astronomy, Michigan State University, East Lansing, MI 48824, USA*
[2.] *Quantum Condensed Matter Division, Oak Ridge National Laboratory, Oak Ridge, TN 37831, USA*
[3.] *Ningbo Institute of Material Technology and Engineering, Chinese Academy of Sciences, Ningbo 315201, China*
[4] *Department of Physics and Engineering Physics, Tulane University, New Orleans, Louisiana 70118, USA*
[5.] *Collaborative Innovation Center of Advanced Microstructures, Laboratory of Solid State Microstructures, School of Physics, Nanjing University, Nanjing 210093, China*
[6.] *NIST Center for Neutron Research, National Institute of Standards and Technology, Gaithersburg, MD 20899, USA*
[7.] *Department of Materials Science and Engineering, University of Maryland, College Park, MD 20742, USA*

We report the hydrostatic pressure-induced electronic and magnetic phase transitions in a Mott insulator, a bilayer ruthenate $Ca_3(Ru_{0.97}Ti_{0.03})_2O_7$, via electronic transport and single crystal neutron diffraction measurements. The system undergoes an insulator-metal transition at a very small hydrostatic pressure ≈ 0.04 GPa followed by a magnetic phase transition around 0.3 GPa, suggesting that the low energy charge fluctuation and magnetic ordering couple to the pressure separately in this compound. *ab* initio calculations show that the suppressed RuO_6 flattening induced by the pressure reduces the orbital polarization and gives rise to an insulator-metal transition preceding the magnetic phase transition.

* Corresponding author: ke@pa.msu.edu

Understanding metal-insulator transition (MIT) in Mott systems arising from strong electron-electron interaction (U) remains a major challenge [1]. Tuning the MIT by means of pressure has been one of the major routes to understand the electronic correlation effect when one assumes an enhanced electronic bandwidth by pressure without change in other physical parameters. However, the strong interplay among various degrees of freedom of lattice, spin, charge, and orbital in many (magnetic) Mott systems often leads to simultaneous variations in crystal structure, magnetism, and electron orbital occupancy, which brings about the complexity in understanding the pressure-induced insulator-metal transition (IMT) [2]. For instance, an application of pressure may alter the transition-metal oxygen octahedral distortion (rotation, tilt, and/or flattening), which can subsequently affect the magnetic exchange interactions and/or the electronic configurations.

Ruthenates with Ruddlesden-Popper type layered structure, $(Sr_{1-x}Ca_x)_{n+1}Ru_nO_{3n+1}$, have been attracting intense attention in the past two decades owing to a wealth of collective phenomena of correlated electrons [3]. For instance, in single-layered ruthenate with $n = 1$, tetragonal Sr_2RuO_4 shows spin-triplet superconductivity [4,5,6], whereas orthorhombic Ca_2RuO_4 is an antiferromagnetic Mott insulator with its MIT temperature $T_{MIT} \sim 360$ K being well above the Neel temperature $T_N \sim 115$ K [7,8]. The orthorhombic distortion in Ca_2RuO_4 originates from RuO_6 octahedral rotation, tilting and flattening, and its MIT mechanism has been a topic of long debate [9,10,11,12,13]. Another distinct characteristic of ruthenates is that their electronic and magnetic properties vary dramatically as the number of RuO layer n increases. This is exemplified by the significant property change from Ca_2RuO_4 to $Ca_3Ru_2O_7$. Unlike Ca_2RuO_4 which shows a G-type AFM order, the bilayer $Ca_3Ru_2O_7$ ($n = 2$) orders antiferromagnetically (AFM) at $T_N \sim 56$ K [14], with ferromagnetic (FM) bilayers stacked in antiparallel alignment

along the *c*-axis (with the spin easy axis along the *a*-axis, denoted as AFM-a) [15,16,17]. This is followed by a MIT with a small increase in resistivity at $T_{MIT} \sim 48$ K [14] as well as a switching of spins to the *b*-axis (denoted as AFM-b) [17], and then by the reappearance of metallicity below 30 K [18] originating from the existence of a small portion of un-nested Fermi surface [19].

Recently, we have shown that partially replacing Ru with ($\geq$ 3%) Ti can also induce a dramatic change of the ground state properties [20,21]: the material turns into a Mott insulator concurrently with a large structural change and a magnetic transition from AFM-a to G-AFM order with the nearest-neighbor spins aligned antiferromagnetically both in-plane and along *c* (Fig. 1b). In the insulating state, the electronic bandwidth of the Ti-substituted compounds becomes narrower compared to that of the pristine compound due to the disruption of carrier hoping by Ti dopants [20], which was confirmed later by photoemission measurements [22]. Interestingly, we found that the 3% Ti-doped compound, $Ca_3(Ru_{0.97}Ti_{0.03})_2O_7$, resides right at the phase boundary [21]: (i) there is only one single phase transition for $Ca_3(Ru_{1-x}Ti_x)_2O_7$ (*x* > 3%) with G-AFM Mott insulating ground state, while for $Ca_3(Ru_{1-x}Ti_x)_2O_7$ (*x* < 3%) there are two phase transitions with the ground state exhibiting localized electronic state and an AFM-b type magnetic structure (Fig. 1b); (ii) at T_{MIT} (~ 46 K) < *T* < T_N (~ 62 K), $Ca_3(Ru_{0.97}Ti_{0.03})_2O_7$ shows a metallic behavior with a magnetic structure similar to that in the pure compound (AFM-a), while it enters a G-AFM Mott insulating state for *T* < T_{MIT}. This suggests that the ground state properties of $Ca_3(Ru_{0.97}Ti_{0.03})_2O_7$ can be sensitive to subtle non-thermal perturbations (i.e., magnetic field and pressure), which may shed light on the entanglement of various of degrees of freedom.

In this paper, we report the pressure-induced phase transitions in the bilayer ruthenate

$Ca_3(Ru_{0.97}Ti_{0.03})_2O_7$ via electronic transport and single crystal neutron diffraction measurements. We show that the electronic structure of this system is extremely sensitive to hydrostatic pressure where an IMT takes place with a very small critical pressure, preceding the magnetic phase transition. The decoupling of IMT and magnetic phase transition with pressure can be attributed to the pressure-induced weakening of oxygen octahedral flattening, which modifies the orbital occupancy and leads to the electronic phase transition.

Figure 1(a) summarizes the temperature (T) - pressure (P) phase diagram of $Ca_3(Ru_{0.97}Ti_{0.03})_2O_7$ established in this work. The associated magnetic structures of various phases denoted in the phase diagram are illustrated in Fig. 1(b). Detailed information on the sample growth and experimental measurements has been discussed in the Supplementary Materials [23]. There are two main features worth emphasizing. First, the electronic structure and the magnetic order couple separately to pressure at low temperature. The system undergoes an IMT with a small critical pressure $P_c \sim 0.04$ GPa, which is followed by the magnetic phase transition from G-AFM to AFM-b with further increasing pressure (~ 0.3 GPa). Second, right below the metallic AFM-a phase at higher temperature, there exists a pressure-induced intermediate magnetic phase with a coexistence of incommensurate AFM (ICM) and AFM-a (or AFM-b) ordering.

The complex T-P phase diagram was established *via* comprehensive electronic transport measurements over a wide range of T and P in conjunction with neutron diffraction measurements. Figure 2(a) shows the temperature dependence of resistivity measured along the c-axis, ρ_c, with various applied hydrostatic pressures. At atmospheric pressure (i.e., $P = 1$ bar = 10^{-4} GPa), ρ_c increases sharply by approximately 6 orders of magnitude at $T_{MIT} \approx 46$ K indicating

a transition to a Mott insulating state [20]. In the presence of hydrostatic pressure, interestingly, ρ_c is dramatically suppressed even with a small pressure. Similarly, the in-plane resistivity ρ_{ab} also significantly decreases upon applying pressure, as shown in the inset of Fig. 2(b). The main panel of Fig. 2(b) presents ρ_c as a function of P measured at $T = 20$ K. One can see that ρ_c drops dramatically and almost saturates above a critical pressure $P_c \approx 0.04$ GPa, suggesting a pressure-induced collapse of the Mott insulating state. Above P_c, both ρ_c and ρ_{ab} exhibit a localized behavior below T_{MIT}, which is in contrast to the quasi-two-dimensional metallic state in the pristine compound. This transport feature is similar to those measured at ambient pressure on $Ca_3(Ru_{1-x}Ti_x)_2O_7$ ($x < 3\%$) [21] and $Ca_3(Ru_{0.95}Fe_{0.05})_2O_7$ [24], and is presumably attributed to disorder scattering upon the transition-metal substitution into Ru sites which destroys the original weakly coherent electronic state arising from the existence of small, non-nested Fermi surface pocket [19]. It is worth noting that the value of P_c for an IMT in $Ca_3(Ru_{0.97}Ti_{0.03})_2O_7$ in this study is much lower than those of other Mott insulators studied thus far. For instance, the critical pressure required to suppress the Mott insulating state is 0.5 GPa for Ca_2RuO_4 [25] and ~ 32 GPa for $LaMnO_3$ [26,27]. This indicates an anomalously high sensitivity of the electronic state in $Ca_3(Ru_{0.97}Ti_{0.03})_2O_7$ to the pressure, which unambiguously testifies to the remarkable sensitivity of the ground state of this material.

To probe the interplay among various degrees of freedom, we also performed single crystal neutron diffraction measurements to explore the pressure effect on both magnetic and crystal structures of $Ca_3(Ru_{0.97}Ti_{0.03})_2O_7$. Figures 3(a, b) show the rocking curves of (0 0 5) and (1 0 2) magnetic Bragg peaks measured on HB3A in High Flux Isotope Reactor (HFIR) at Oak Ridge National Laboratory (ORNL) at $T = 4$ K with $P = 10^{-4}$ GPa and 0.85 GPa. A CuBe clamp cell with Fluorinert (FC70) as the pressure medium was used [23]. Note that the (0 0 5) Bragg peak

refers to the AFM-b or AFM-a type magnetic structures in $Ca_3Ru_2O_7$ [17] while (1 0 2) to the G-AFM magnetic structure in the Ti-doped $Ca_3Ru_2O_7$ [20]. Compared with the zero pressure data, surprisingly, we find that at P = 0.85 GPa the (1 0 2) Bragg peak disappears (Fig. 3b) while the (0 0 5) Bragg peak emerges (Fig. 3a), which indicates a magnetic phase transition from the G-AFM to the AFM-b type order [23].

Temperature dependence of the magnetic Bragg peaks, (0 0 5) and (1 0 2), is plotted in Fig. 3(c). At P = 10^{-4} GPa, the (0 0 5) Bragg peak appears at T_N = 62 K corresponding to the AFM-a order, followed by its disappearance and an emergence of the (1 0 2) Bragg peak below T_{MIT} = 46 K associated with the G-AFM order, which is consistent with the previous study [20]. In contrast, at P = 0.85 GPa the intensity of (1 0 2) Bragg peak is completely suppressed for the whole measured temperature range; Instead, the (0 0 5) Bragg peak emerges below $T_{MIT} \approx$ 38 K, confirming the pressure-induced magnetic phase transition. In comparison with the zero pressure case, the change of magnetic structure correlates with the much smaller enhancement in resistivity observed below T_{MIT} shown in Fig. 2(a) and the inset of Fig. 2(b). Note that both T_{MIT} and T_N decrease in the presence of pressure. Furthermore, one can see that at 31 K < T < 38 K there is a V-shaped drop in intensity of the pressure-induced (0 0 5) Bragg peak, indicating an additional magnetic phase induced by the applied pressure. This is corroborated by an intermediate region between T^* and T_{MIT} in the transport measurements (Fig. 2c) where T^* marks the kink points in the resistivity curves. We find that in this region the system displays a coexistence of commensurate AFM-a (or AFM-b) and incommensurate magnetic phases which are represented by the (0 0 5) and (H 0 5) (H $\approx \pm$ 0.022) peaks, respectively, as shown in Fig. 3(d) [23].

To further explore the evolution of the magnetic structure as a function pressure, especially at low pressure region, we performed neutron diffraction measurements using He gas pressure cell on the BT7 triple-axis spectrometer at NCNR at NIST to gain a better pressure control [23]. Figure 4(a) shows scans of (1 0 2) and (0 0 5) magnetic Bragg peaks at lower pressure values. Interestingly, one can see that G-AFM order persists for pressure up to 0.2 GPa, at which the electronic structure transition (i.e., IMT) already occurs (Fig. 2). The magnetic structure transforms to the AFM-b type for $P > 0.3$ GPa. This suggests that the electronic structure and magnetic order couple separately with pressure, with the magnetic phase transition preceded by the IMT upon applying a pressure. Such a feature is in sharp contrast to the case when varying temperature [20].

The hydrostatic pressure effect on the physical properties of $Ca_3(Ru_{0.97}Ti_{0.03})_2O_7$ is summarized via the T-P phase diagram presented in Fig. 1. It is known that, due to the extended nature of the 4d orbital of Ru^{4+} ions, the magnetic and electronic properties of ruthenates are very sensitive to the structural distortion (i.e., octahedral rotation, tilt, and / or flattening), which leads to a variation of the t_{2g} orbital degeneracy. For instance, an enhanced flattening of RuO_6 octahedra along the c-axis is anticipated to lift the degeneracy of three t_{2g} bands with the d_{xy} orbital more energetically favorable, resulting in an antiferromagnetic insulating state [28]. Generally, the octahedral distortion can be efficiently altered by either internal pressure via chemical substitution or external pressure, as elucidated in $(Sr_{1-x}Ca_x)_2RuO_4$ [25,29,30,31,32]. Thus, it is appealing to investigate the response of the crystal structure to pressure and its interplay with the magnetic and electronic properties in $Ca_3(Ru_{0.97}Ti_{0.03})_2O_7$.

Figure 4(c) shows the non-monotonic dependence of lattice parameter c on pressure. c

increases first with pressure and reaches a maximum at a pressure of ~ 0.3 GPa, which is much larger than P_c for the IMT but is close to the value where there is a magnetic phase transition from G-AFM to AFM-b. This implies a pressure-induced anisotropic structural distortion (instead of regular lattice contraction) a feature similar to what was observed in Ca_2RuO_4 [29]. With further increase of pressure, c decreases as a result of normal compression.

To further understand the mechanism of the pressure-induced magnetic and electronic properties, we performed first-principles calculations using local density approximation (LDA)+U method with a moderate U of 2 eV [33]. The irreducible Brillouin zone was sampled with 100 k-points. Since the Ti induced change in electron count is expected to be very small, the calculations were done for the parent $Ca_3Ru_2O_7$. Figure 5(a) shows the projected density of states (PDOS) of Ru t_{2g} bands (d_{xy} and d_{xz}/d_{yz}) calculated for the G-AFM state using the experimental structure determined at $T = 4$ K in the absence of external pressure. In contrast to the metallic phase obtained previously without taking into account U [20], an electronic gap ~ 0.2 eV develops for all t_{2g} bands, affirming the important role of the electron correlation in this system. Interestingly, one can see that in the spin-down channel the xy orbital is almost fully occupied while the xz/yz orbitals are nearly empty, which suggests an electronic configuration of xy (↑↓) xz/yz (↑,↑) bands for the G-AFM insulating phase [34]. Such orbital polarization is ascribed to the flattening of RuO_6 octahedra, which causes the xy orbital to be shifted downward. In Ca_2RuO_4, similar orbital polarization has been observed [10,12]. The flattening of RuO_6 can be roughly described by d_1/d_2, where d_1 (d_2) is the Ru-O bond length along the c-axis (in-plane) direction (inset of Fig. 5b). Without external pressure, the extracted d_1/d_2 is ~ 0.985 for the G-AFM phase.

In order to qualitatively capture the pressure-induced metallic state with G-AFM spin structure, we calculated the band structure with various ratios of d_1/d_2 but keeping the magnetic

8

order the same. Note that under non-zero pressure, since the detailed atomic parameters are unknown, d_1/d_2 values are changed by assuming constant crystal volume with an increase (decrease) in c (b) as reported previously in the temperature dependent study [20]. Thus, d_1/d_2 increases with P for $P \leq 0.3$ GPa as a result of the suppression of RuO_6 octahedral flattening (Fig. 4c). Figure 5(b) presents the calculated band gap as a function of d_1/d_2. As d_1/d_2 increases, the band gap decreases and vanishes for larger d_1/d_2, indicating an IMT which is consistent with our experimental results. The PDOS of the pressure-induced metallic state for $d_1/d_2 = 1.02$ is shown in Fig. 5(c). It is seen that under higher pressure the occupancy of the xy orbital in the spin-down channel is largely decreased, indicating the absence of orbital polarization. Future experimental studies to examine the orbital configuration of this system are warranted.

In conclusion, we have reported the hydrostatic pressure-induced electronic and magnetic phase transitions in $Ca_3(Ru_{0.97}Ti_{0.03})_2O_7$. We find that the electronic structure and magnetic order of this material are highly sensitive and couple separately to pressure, which is evidenced by the occurrence of an IMT followed by a change of magnetic structure as the pressure increases. First-principles calculations show that the pressure-induced suppression of the flattening of the RuO_6 octahedra reduces the orbital polarization and leads to the IMT without changing the magnetic structure. This work highlights the remarkable magnetic and electronic instabilities of the ground state of this system and the significance of strong interplay among various degrees of freedom in controlling materials properties.

Figure Captions

Figure 1. (a) Temperature (T) – pressure (P) phase diagram of $Ca_3(Ru_{0.97}Ti_{0.03})_2O_7$. Blue dots represent T_N values, red dots for T_{MIT}, and black ones for T^* extracted from the electronic transport measurements. (b) Schematics of spin structures of AFM-a with spin direction along the a-axis, G-AFM with nearest-neighbor spins antiparallel aligned, and in-plane view of the incommensurate (ICM) ordering. The green dashed frame represents the in-plane projection of the repeating unit cell. Note the spin structure of AFM-b is similar to AFM-a but with spins pointing along the b-axis.

Figure 2. (a) Temperature dependence of the out-of-plane resistivity ρ_c measured at various hydrostatic pressures. (b) Pressure dependence of ρ_c at $T = 20$ K extracted from (a). Inset shows the in-plane resistivity ρ_{ab} (T). (c) An expanded view of ρ_c (T) above the critical pressure. Arrows point to T^* associated with the incommensurate magnetic phase. Error bars in all figures represent one standard deviation.

Figure 3. Rocking curves of the (0 0 5) magnetic Bragg peak representing AFM-a or AFM-b type spin structure (a) and (1 0 2) magnetic Bragg peak representing G-AFM spin structure (b) measured under $P = 10^{-4}$ GPa (i.e, atmospheric pressure) and 0.85 GPa. Measurement temperature $T = 4$ K. (c) Temperature dependence of (0 0 5) and (1 0 2) magnetic Bragg peak intensities measured at $P = 10^{-4}$ GPa and 0.85 GPa. T_N (green dashed line) and T_{MIT} (blue dashed line) refer to the Neel temperature and metal-insulator transition at the ambient pressure, respectively. The neutron counting time for each curve (i.e., 120s, 60s, or 30s) is denoted. (d) T – (H 0 5) contour map measured at $P = 0.85$ GPa showing the occurrence of an incommensurate magnetic ordering in the intermediate temperature regime.

Figure 4. (H 0 5) scan (a) and θ-2θ scan of (1 0 2) magnetic Bragg peak (b) measured at 4 K under various pressures. (c) Pressure dependence of lattice parameter c measured at 4 K.

Figure 5. (a, b) Calculated partial density of states (PDOS) of Ru t_{2g} orbitals (*xy* and *xz/yz*) with G-AFM magnetic structure under two different pressures as indicated by d_1/d_2 values. d_1 (d_2) refers to the Ru-O bond length along the *c*-axis (in-plane) direction as illustrated in the inset. (c) Calculated electronic band gap as a function of d_1/d_2 showing a pressure-induced insulator-to-metal transition.
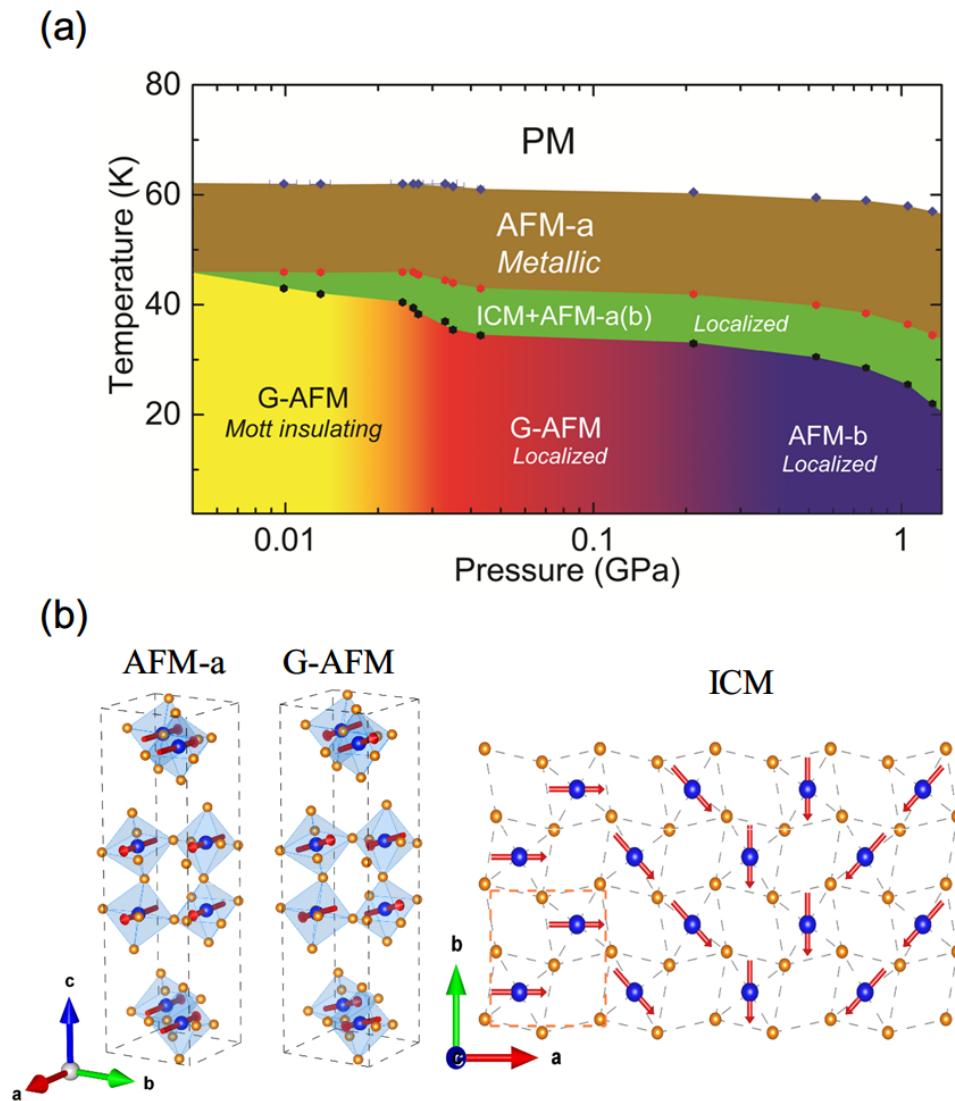
Figure 1.

(a)

(b)
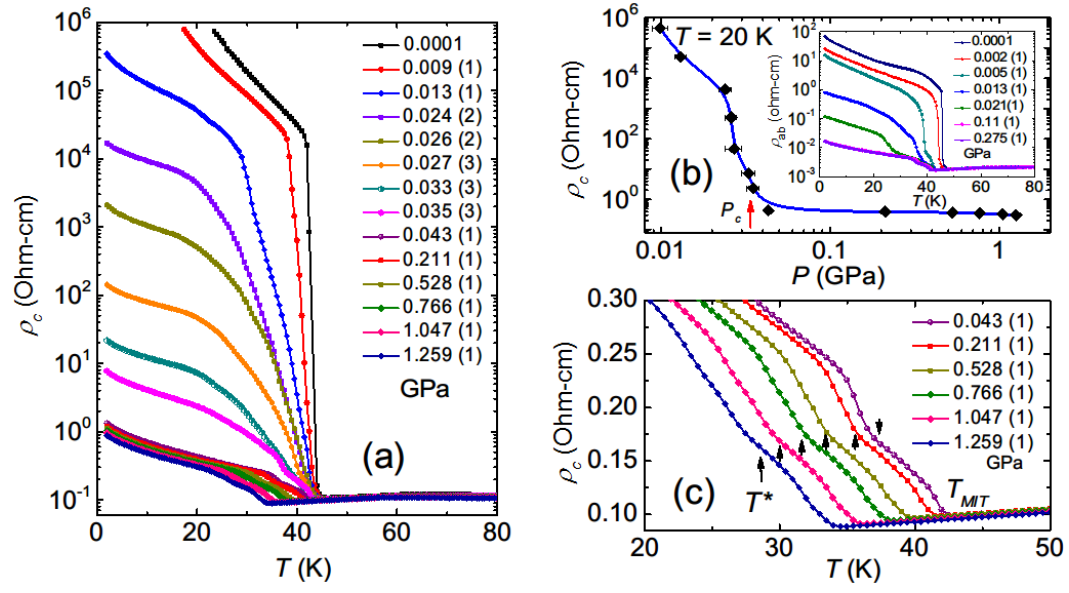
AFM-a   G-AFM   ICM
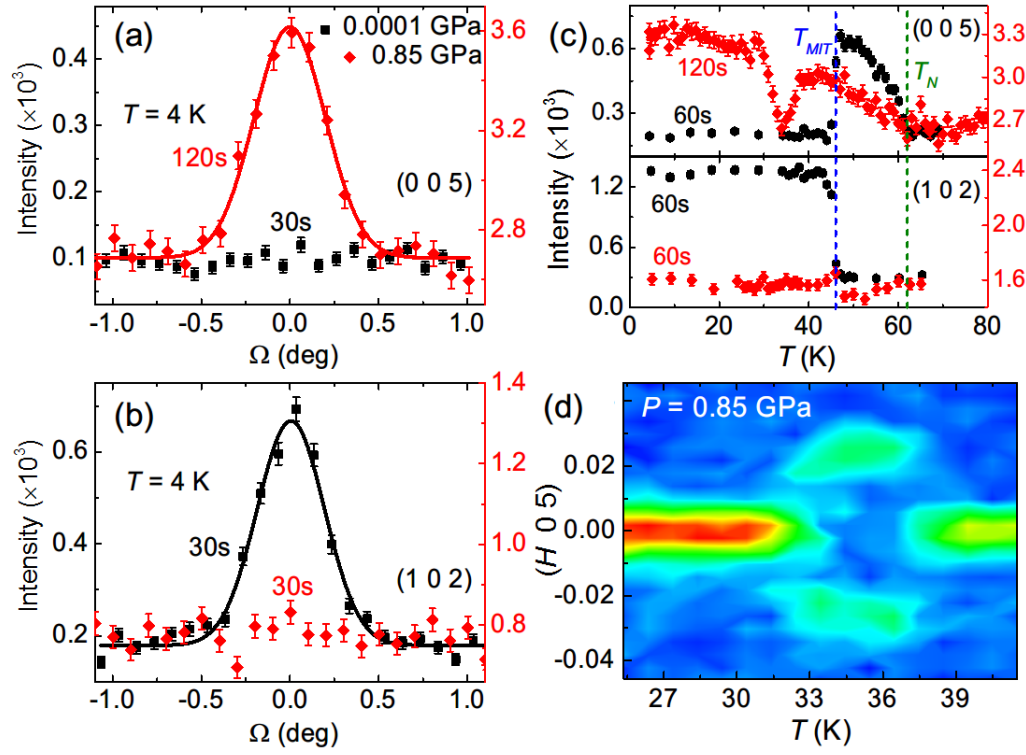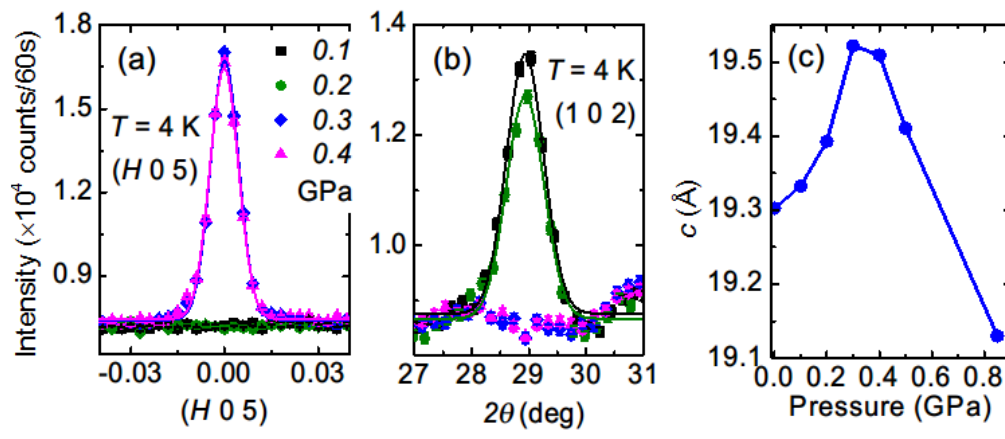
Figure 2.
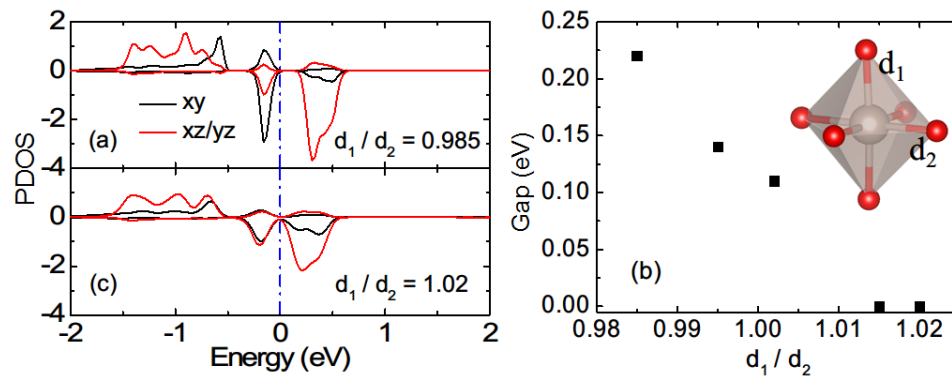
Figure 3.

Figure 4.

Figure 5.

[1] M. Imada, A. Fujimori, and Y. Tokura, Reviews of Modern Physics **70** (4), 1039 (1998).

[2] E. Dagotto and Y. Tokura, MRS Bulletin **33** (11), 1037 (2008).

[3] C. Noce, A. Vecchione, M. Cuoco, and A. Romano, Springer (2002).

[4] Y. Maeno, H. Hashimoto, K. Yoshida, S. Nishizaki, T. Fujita, J. G. Bednorz, and F. Lichtenberg, Nature **372** (6506), 532 (1994).

[5] G. M. Luke, Y. Fudamoto, K. M. Kojima, M. I. Larkin, J. Merrin, B. Nachumi, Y. J. Uemura, Y. Maeno, Z. Q. Mao, Y. Mori, H. Nakamura, and M. Sigrist, Nature **394** (6693), 558 (1998).

[6] K. Ishida, H. Mukuda, Y. Kitaoka, K. Asayama, Z. Q. Mao, Y. Mori, and Y. Maeno, Nature **396** (6712), 658 (1998).

[7] G. Cao, S. McCall, M. Shepard, J. E. Crow, and R. P. Guertin, Phys Rev B **56** (6), R2916 (1997).

[8] S. Nakatsuji, S. I. Ikeda, and Y. Maeno, Journal of the Physical Society of Japan **66** (7), 1868 (1997).

[9] V. I. Anisimov, I. A. Nekrasov, D. E. Kondakov, T. M. Rice, and M. Sigrist, European Physical Journal B **25** (2), 191 (2002).

[10] Z. Fang, N. Nagaosa, and K. Terakura, Phys Rev B **69** (4), 045116 (2004).

[11] J. H. Jung, Z. Fang, J. P. He, Y. Kaneko, Y. Okimoto, and Y. Tokura, Physical Review Letters **91** (5), 056403 (2003).

[12] E. Gorelov, M. Karolak, T. O. Wehling, F. Lechermann, A. I. Lichtenstein, and E. Pavarini, Physical Review Letters **104** (22), 226401 (2010).

[13] G. Q. Liu, Phys Rev B **84** (23), 235136 (2011).

[14] G. Cao, S. McCall, J. E. Crow, and R. P. Guertin, Physical Review Letters **78** (9), 1751 (1997).

[15] Y. Yoshida, S. I. Ikeda, H. Matsuhata, N. Shirakawa, C. H. Lee, and S. Katano, Phys Rev B **72** (5), 054412 (2005).

[16] D. J. Singh and S. Auluck, Physical Review Letters **96** (9), 097203 (2006).

[17] W. Bao, Z. Q. Mao, Z. Qu, and J. W. Lynn, Physical Review Letters **100** (24), 247203 (2008).

[18] Y. Yoshida, I. Nagai, S. I. Ikeda, N. Shirakawa, M. Kosaka, and N. Mori, Phys Rev B **69** (22), 220411 (2004).

[19] F. Baumberger, N. J. C. Ingle, N. Kikugawa, M. A. Hossain, W. Meevasana, R. S. Perry, K. M. Shen, D. H. Lu, A. Damascelli, A. Rost, A. P. Mackenzie, Z. Hussain, and Z. X. Shen, Physical Review Letters **96** (10), 107601 (2006).

[20] X. Ke, J. Peng, D. J. Singh, T. Hong, W. Tian, C. R. Dela Cruz, and Z. Q. Mao, Phys Rev B **84** (20), 201102 (2011).

[21] J. Peng, X. Ke, G. C. Wang, J. E. Ortmann, D. Fobes, T. Hong, W. Tian, X. S. Wu, and Z. Q. Mao, Phys Rev B **87** (8), 085125 (2013).

[22] S. Tsuda, N. Kikugawa, K. Sugii, S. Uji, S. Ueda, M. Nishio, and Y. Maeno, Phys Rev B **87** (24), 241107 (2013).

[23] Supplementary Materials.

[24] X. Ke, J. Peng, W. Tian, T. Hong, M. Zhu, and Z. Q. Mao, Phys Rev B **89** (22), 220407 (R) (2014).

[25] F. Nakamura, T. Goko, M. Ito, T. Fujita, S. Nakatsuji, H. Fukazawa, Y. Maeno, P. Alireza, D. Forsythe, and S. R. Julian, Phys Rev B **65** (22), 220402 (2002).

[26] I. Loa, P. Adler, A. Grzechnik, K. Syassen, U. Schwarz, M. Hanfland, G. K. Rozenberg, P. Gorodetsky, and M. P. Pasternak, Phys Rev Lett **87** (12), 125501 (2001).

[27] M. Baldini, T. Muramatsu, M. Sherafati, H. K. Mao, L. Malavasi, P. Postorino, S. Satpathy, and V. V. Struzhkin, Proc Natl Acad Sci U S A **112** (35), 10869 (2015).

[28] Z. Fang and K. Terakura, Phys Rev B **64** (2), 020509 (2001).

[29] P. Steffens, O. Friedt, P. Alireza, W. G. Marshall, W. Schmidt, F. Nakamura, S. Nakatsuji, Y. Maeno, R. Lengsdorf, M. M. Abd-Elmeguid, and M. Braden, Phys Rev B **72** (9), 094104 (2005).

[30] S. Nakatsuji and Y. Maeno, Physical Review Letters **84** (12), 2666 (2000).

[31] S. Nakatsuji and Y. Maeno, Phys Rev B **62** (10), 6458 (2000).

[32] O. Friedt, M. Braden, G. Andre, P. Adelmann, S. Nakatsuji, and Y. Maeno, Phys Rev B **63** (17), 174432 (2001).

[33] H. T. Dang, J. Mravlje, A. Georges, and A. J. Millis, Phys Rev B **91** (19) (2015).

[34] M. Zhu, J. Peng, T. Zou, K. Prokes, S. D. Mahanti, T. Hong, Z. Q. Mao, G. Q. Liu, and X. Ke, Phys. Rev. Lett. **116**, 216401 (2016).